Date of Report: 03/12/2024

Date of Experiment: 12/11/2024

Investigating the Zeeman effect and Obtaining the ratio of Elementary Charge and Mass of an Electron

Experiment Conducted by: Neeraj Nandan Akella

Lab Partner: Sam Patel-Espin

Abstract

In this report, the Zeeman effect was produced for a Cadmium lamp in presence of a magnetic field, observed using a set of optical elements and a Fabry-Perot Etalon, to study its characteristics and find the ratio of elementary charge with mass of an electron. The experiment involved three parts: Calibration of the magnetic field, Zeeman effect in transverse configuration and in longitudinal configuration.

The second part allowed for the calculation of the ratio by analysing the distances between Zeeman components from the images taken at different strengths of the magnetic field. From two different methods of analysing the images, the value of highest accuracy of the ratio (error of 1.4%) was found to be $(1.78 \pm 0.05) \times 10^{11}\ Ckg^{-1}$ where the theoretical value lies within one standard deviation. However, the experiment still contained various sources of errors as this value was only obtained from constraining the data to a linear curve with an intercept set to zero.

1. Introduction

This experiment aims to investigate the visual characteristics of the Zeeman effect and calculate the ratio of electron charge and mass of an electron. The Zeeman effect is a phenomenon which describes the splitting of spectral lines of atomic energy levels in the presence of an external magnetic field. H. A. Lorentz first predicted this effect in 1895 and P. Zeeman confirmed it experimentally [1].

In this investigation, the normal Zeeman effect is the primary focus, which is characterized as the spectral line splitting into just three components (when spin is zero, S = 0) [2]. When there is no magnetic field present, the separation between the nearby energy levels is negligible, hence only one spectral line is observed. In the presence of a magnetic field the energy levels of the electron are separated more causing the Zeeman effect. These energy levels can be derived from the magnetic moment of the electron which allows to quantify the separation of the Zeeman components.

The magnetic moment ($\boldsymbol{\mu}$) and its energy (E) are given by [1]:

$$\boldsymbol{\mu} = \frac{\mu_B}{\hbar}\boldsymbol{J} \tag{1}$$

$$E = -\boldsymbol{\mu} \cdot \boldsymbol{B} \tag{2}$$

Where $\hbar$ is the reduced Planck's constant, $\boldsymbol{J}$ is the total angular momentum ($\boldsymbol{J} = \boldsymbol{L}$ for zero spin), $\boldsymbol{B}$ is the external magnetic field and μ_B is Bohr's magneton, given by:

$$\mu_B = -\frac{\hbar e}{2m_e} \tag{3}$$

The magnitude of $\boldsymbol{J}$ in the direction of $\boldsymbol{B}$ is given by:

$$J_z = M_J \hbar \tag{4}$$

Where M_J is a quantum number with values $M_J = J, J-1, J-2, \ldots -J$

Equation (4) shows the splitting of angular momentum into multiple Zeeman components each differing by M_J. This allows to rewrite equation (3) and find the energy interval between M_J, M_{J+1}:

$$E = \mu_B M_J B$$

$$\Delta E = \mu_B B \tag{5}$$

The frequency difference between the components is given by [3]:

$$\Delta\nu = \pm\frac{\Delta E}{h}$$

$$\Delta\nu = \frac{eB}{4\pi m_e} \tag{6}$$

In this experiment, a Cadmium lamp was used which emits a red spectral line (with a wavelength $\lambda_0 = 643.8\,nm$ and frequency $f_0 = 465.7\,THz$) which corresponds to the transition $5\,D_2^1(J = 2, S = 0) \longrightarrow 5\,P_1^1(J = 1, S = 0)$ [4]:

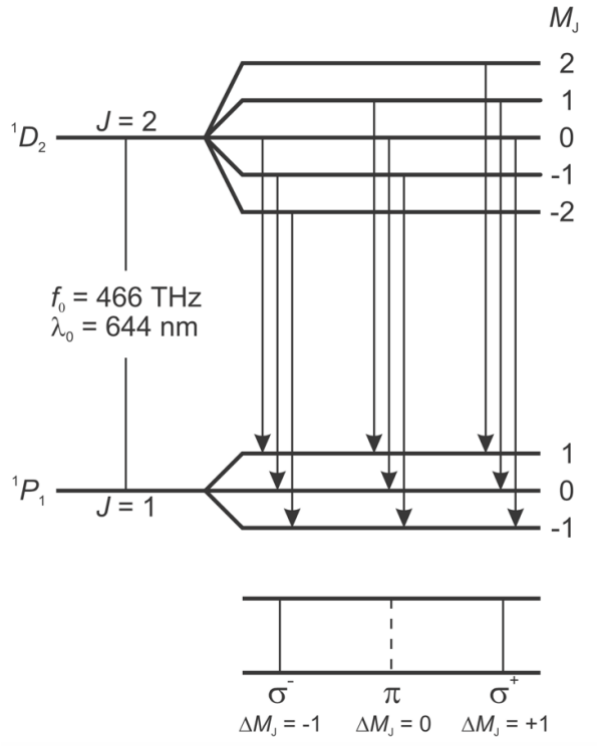

Figure 1: Electron transitions of Cadmium causing normal Zeeman effect (diagram from [1]).

As seen in figure 1, the Zeeman effect for Cadmium includes two σ lines and a π line corresponding to $M_J = \pm 1$ and 0 respectively.

To observe the Zeeman effect, an optical component, Fabry-Perot Etalon, is used which splits incoming light into concentric circles. The interferometer uses two parallel surfaces to create multiple beams where the condition for constructive interference is given by [5]:

$$2nd\,\cos\theta = k\lambda \tag{7}$$

$$2nd \approx k\lambda \tag{8}$$

Where n is the refractive index and d is the thickness of the etalon, θ is the angle of incidence, λ is the wavelength of incident light and k is order of interference. For near normal incidence equation (7) simplifies to equation (8).

Equation (8) can be rearranged to find $\Delta\nu$ in terms of Δk:

$$\frac{2nd\nu}{c} = k$$

$$\Delta k = \frac{2nd\Delta\nu}{c}$$

$$\Delta k = \frac{dneB}{2\pi c m_e} \tag{9}$$

Using this optical component, the Zeeman effect can be observed as a series of triplet concentric circles (in transverse configuration) or a series of doublets (in longitudinal configuration):

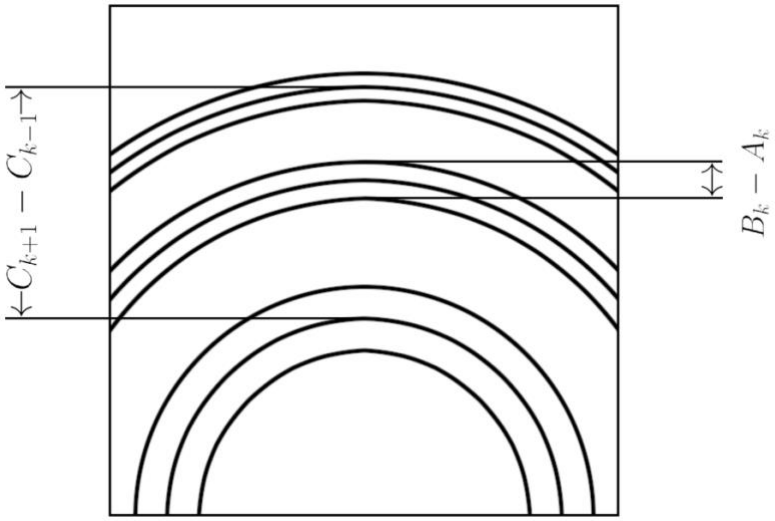

Figure 2: Visualization of Δk ratio given by the Zeeman components in transverse configuration.

From this Δk can be defined with the relative distances of the concentric circles [1]:

$$\Delta k = \frac{B_k - A_k}{C_{k+1} - C_{k-1}} \tag{10}$$

Hence, the ratio $\frac{e}{m_e}$ can be calculated using equation (9) and (10).

2. Methods

For this investigation, multiple optical components were used, configured on an optical bench in the following way:

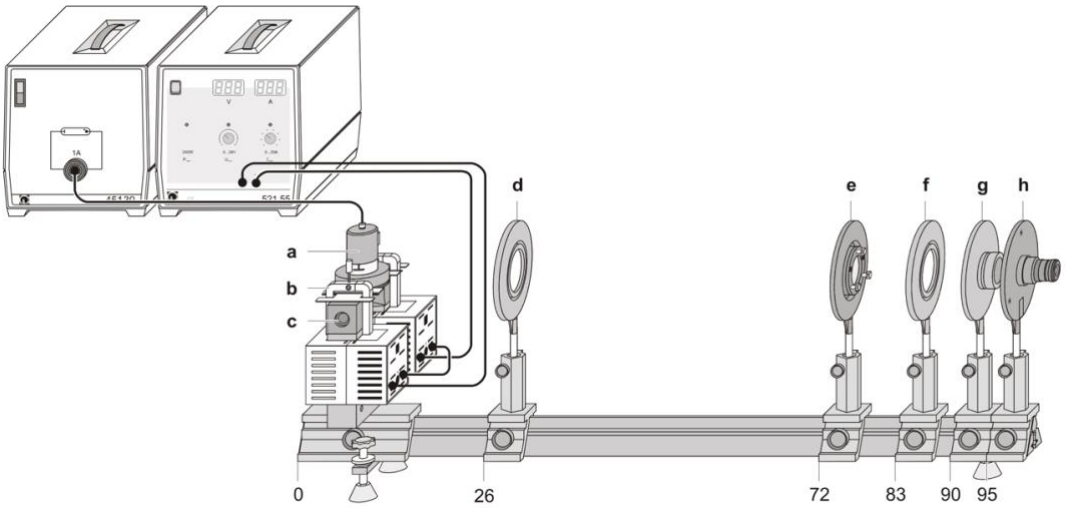

Figure 3: Transverse configuration for Zeeman effect. The position of each optical component is given in cm (left edge). (**a**) Cadmium lamp with holding plate, (**b**) Clamps, (**c**) Pole pieces, (**d**) Positive lens, f = 150 mm (condenser lens), (**e**) Fabry-Perot etalon, (**f**) Positive lens, f = 150 mm (imaging lens), (**g**) Colour filter (red) in holder, (**h**) Ocular with line graduation (diagram and material labels from [6]).

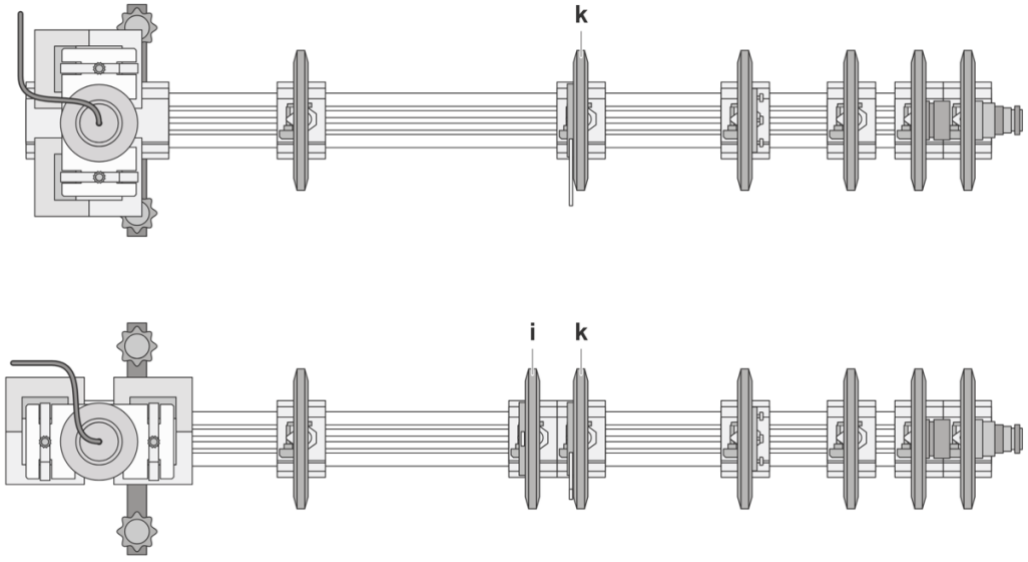

Figure 4: Transverse and Longitudinal configuration (top and bottom respectively) for Zeeman effect from above. (**i**) Quarter-wavelength plate, (**k**) Polarization filter (diagram and material labels from [6]).

In the first part of the investigation, the Cadmium lamp was removed, and a hall probe was placed in between the pole pieces. This allowed to calibrate the current supplied to the pole pieces with the resulting magnetic field. The current was varied from 0.0 to 3.0 A, however, the increments were not constant as the dial used to change the current supply was highly sensitive, preventing to meaningfully change the current at constant increments while having enough data point for calibration.

After the calibration stage, the hall probe was removed, and the Cadmium lamp was mounted between the pole pieces once again (while the circuit was turned off). The exposed part of the cadmium lamp was facing the optical bench to have a transverse configuration while no polarizer was placed on the bench (top of figure 4).

After the lamp has heated up, a camera was placed at the end of the optical bench, directed towards the ocular with line graduations. The Fabry-Perot etalon was tilted until a high contrast image was produced on the camera. The current was then switched on and increased until the Zeeman effect was observed. A few pictures were taken with all three lines (triplet) visible at once.

A polarizer was then placed on the optical bench to observe the π and σ lines individually. When the polarizer was at an angle of 0 degrees, σ lines (pair of close concentric circles) were observed and when the polarizer was at an angle of 90 degrees, π lines (single concentric circles) were observed:

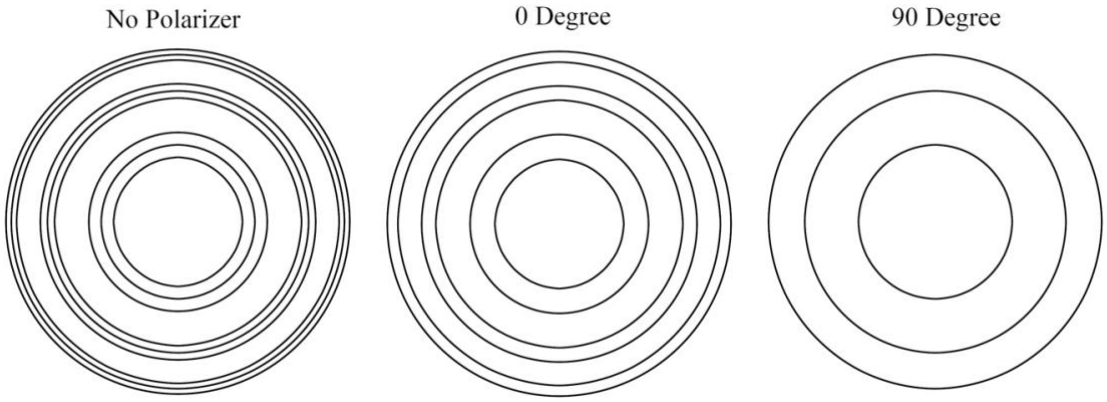

Figure 5: Visualisation of Zeeman components in transverse configuration with polarizer angles when B > 0.

The current was varied from 4.0 to 8.5 A (the current was increased from 3 A since the Zeeman effect was not visible within that range) at increments of 0.5 A, and images of the resulting π and σ lines were taken, and their file names noted (while changing the polarizer angle from 0 to 90 degrees between pictures).

The current was switched off once again and the coils and pole pieces were rotated to match the longitudinal setup (bottom of figure 4). A quarter-wave plate was placed while the polarizer was removed to observe the circularly polarized σ line components from the Zeeman effect. The current was switched on and few images were taken with the pair of lines visible. The polarizer was then added to the optical bench. When the polarizer was at 0 degrees, both σ lines were visible and at 45 degrees, only one of the σ lines was visible (the one with smaller radius):

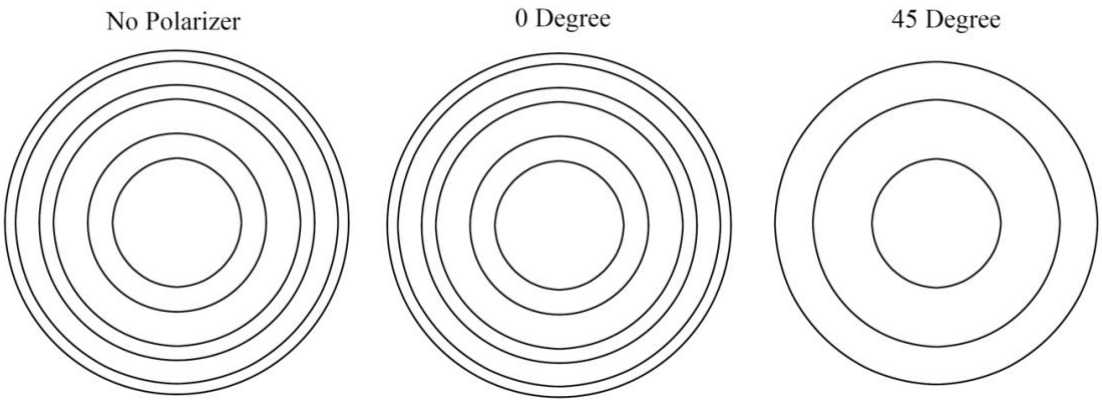

Figure 6: Visualisation of Zeeman components in longitudinal configuration with polarizer angles when B > 0.

Similar to the previous part, the current was varied from 4.0 to 5.5 A at constant increments of 0.5 A and the images of the Zeeman components were taken and their names noted (while changing the polarizer angle from 0 to 45 degrees between each image).

3. Results

The results of each section of the experiment are presented below.

I Calibration of the Magnetic Field

The calibration of the magnetic field produced a linear curve:

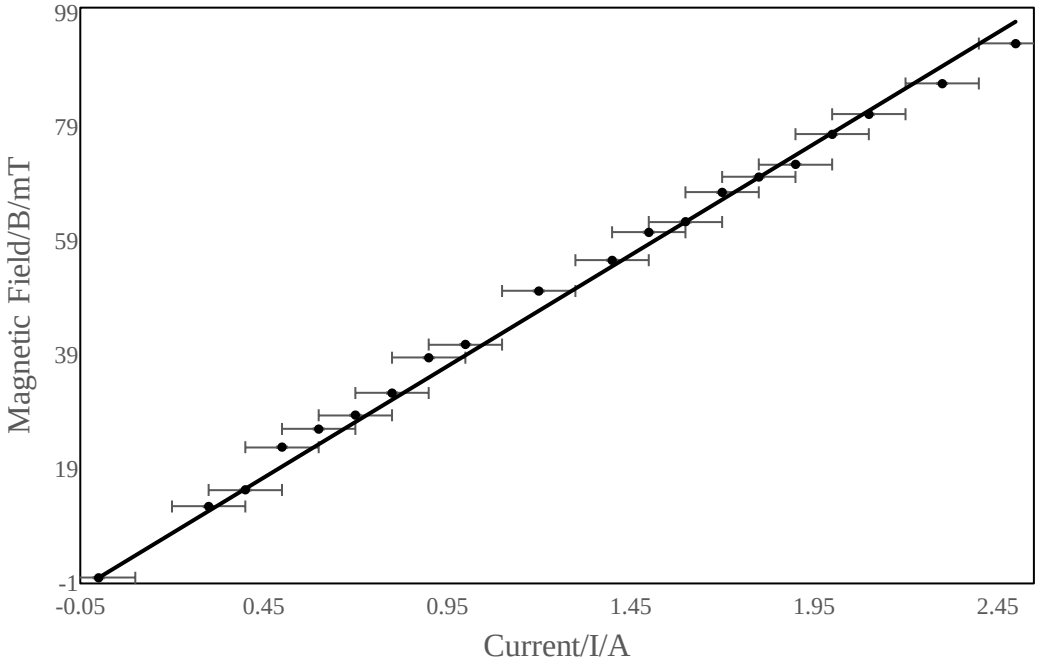

Figure 7: Results from part 1 of the experiment plotted as a linear curve. The best fit line is fitted to zero intercept with equation B = (39.0 ± 0.3) I and R^2 = 0.9987 (vertical error bars drawn but not visible).

The high regression value in figure 7 (calculated using linest on excel) indicates a strong correlation between the current and magnetic field. Hence the above figure was used to extrapolate the values of the magnetic field for the next parts of the experiment with the best fit line equation.

The equation was found through linest (including the uncertainty in slope) while setting the intercept to zero since the data itself has an origin point (0A, 0mT) and is supposed to calibrate the magnetic field for different values of current. The error in current and magnetic field (± 0.1 A and ± 0.1 mT respectively) were obtained from the least count of the instruments used to measure them.

For the second part of the experiment, two methods were used to determine Δk. One involved finding the pixel distances between the lines in the images and the other involved using the graduations visible on the image from the ocular:

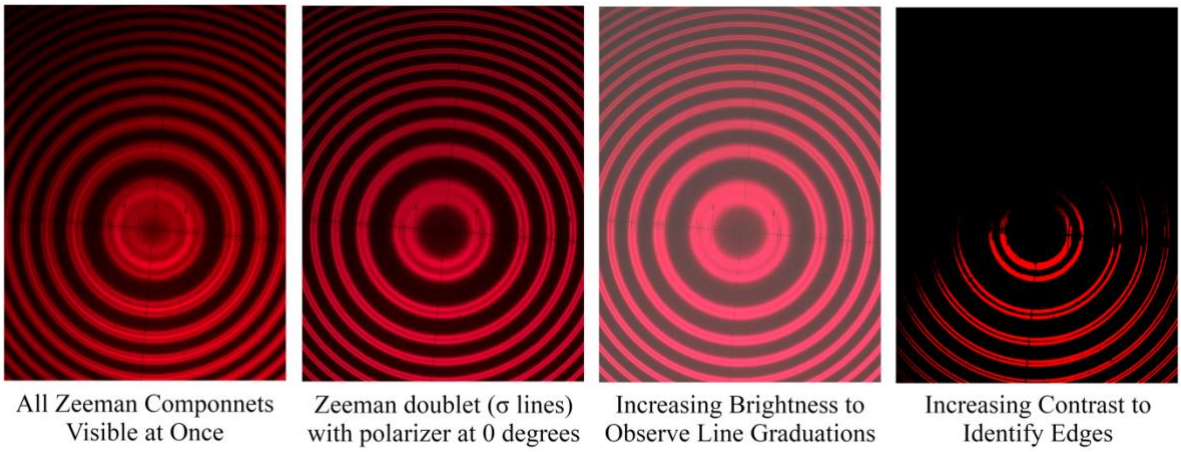

Figure 8: Overview of the images taken in transverse configuration and methods used to analyse the Zeeman components.

By increasing the brightness, the line graduations could be measured (which had increments of 0.1 mm, giving an uncertainty of ± 0.05 mm). By increasing the contrast of the image, the edges of the concentric lines could be observed clearly (this enhancement could not be used for the graduations since they become invisible under the process) which allowed for the pixel measurements between the concentric circles.

II Data from Line Graduations

Since the graduations on the left and right side of the image were harder to observe, the values for Δk from only the first 3 sets of lines were measured (k = 2, C_1, C_3, A_2, and B_2 using the naming convention of figure 2). The resulting data was plotted against magnetic field B which was calculated using the best fit line equation from figure 7:

$$B = mI \tag{11}$$

$$\Delta B = B\sqrt{\left(\frac{\Delta m}{m}\right)^2 + \left(\frac{\Delta I}{I}\right)^2} \tag{12}$$

Where m and Δm are the slope and its uncertainty from figure 7.

Similarly, the uncertainty in Δk is given by:

$$\Delta' \Delta k = \Delta k \sqrt{\left(\frac{Q}{\Delta \sigma}\right)^2 + \left(\frac{Q}{\Delta \pi}\right)^2} \tag{13}$$

Where $\Delta \sigma = B_k - A_k$, $\Delta \pi = C_{k+1} - C_{k-1}$ and Q is the quadrature sum of the uncertainty of the line graduations (± 0.07 mm). Δ' was used for uncertainty to differentiate from Δk.

The resulting data is plotted below:

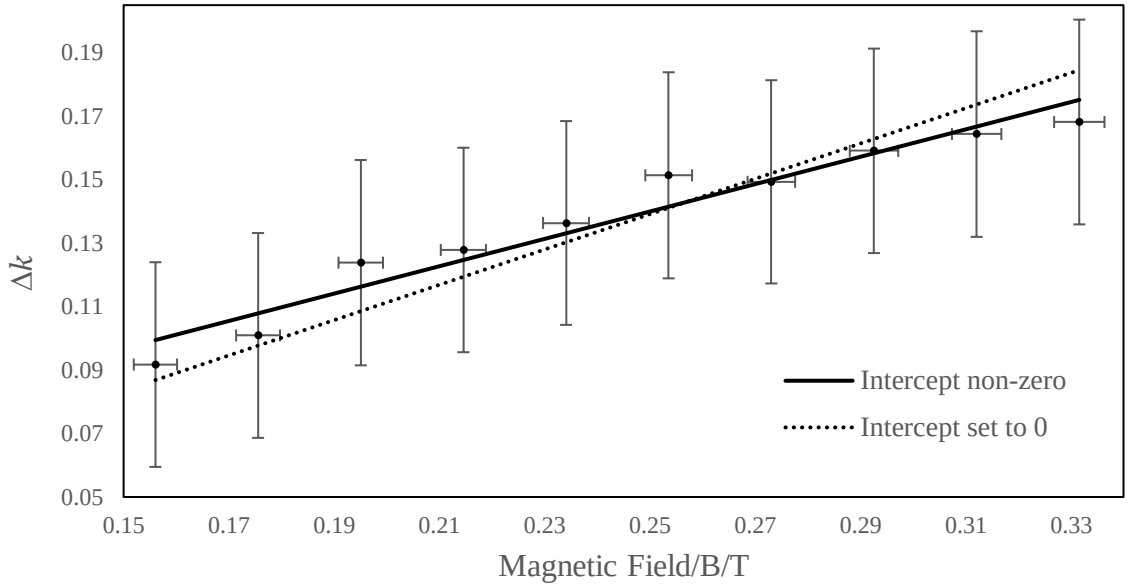

Figure 9: Data obtained from the line graduations (k = 2) plotted with Fractional Order Splitting (Δk) against Magnetic Field Strength. The two best fit lines were plotted with intercept fixed to 0 and not fixed, having R^2 = 0.9956 and R^2 = 0.9452 respectively.

In figure 9 it is visible that the vertical horizontal bars are extremely large which arises due to the significantly high uncertainty present in the line graduation method. This effect is visible in the data values themselves, as some of the values seem to not follow the trend line or have similar values (forming a sort of step). The data values also required some guesswork, as the change in the pattern was smaller than the least count as well.

For this data, two best fit lines were drawn, one with an intercept fixed to zero ($b = 0$) to match equation (9). The best fit line equations were calculated using linest:

$$\Delta k = (0.43 \pm 0.04)B + (0.032 \pm 0.009)$$

$$\Delta k_{b=0} = (0.557 \pm 0.012)B$$

The ratio of $\frac{e}{m_e}$ was calculated from the slope for both versions of the best fit line:

$$\frac{e}{m_e} = (1.40 \pm 0.12) \times 10^{11}\ Ckg^{-1}$$

$$\left(\frac{e}{m_e}\right)_{b=0} = (1.80 \pm 0.04) \times 10^{11}\ Ckg^{-1}$$

The value and its uncertainty were calculated using equation (14) and (15):

$$a = \frac{dn}{2\pi c}\frac{e}{m_e}$$

$$\frac{e}{m_e} = \frac{2\pi ca}{dn} \tag{14}$$

$$\Delta\left(\frac{e}{m_e}\right) = \frac{e}{m_e}\left(\frac{\Delta a}{a}\right) \tag{15}$$

Where a and Δa are the slope and its uncertainty ($d = 4mm, n = 1.457$ are the thickness and refractive index of the etalon [7], $c = 299\,792\,458\,ms^{-1}$ [8])

It is seen that the second value of the ratio when the intercept was set to 0 is more accurate and has an error of 2.3% using the theoretical value of $\frac{e}{m_e} = 1.759 \times 10^{11}\,Ckg^{-1}$ [8]. The percentage error was calculated using:

$$\%Error = \frac{|Theo - Exp|}{Theo} \times 100 \tag{16}$$

III Data from Pixel Measurements

The same analysis was conducted with the second method of using pixel measurements, where the uncertainty in this method was much smaller when taken as least count of the tool measuring in pixels. Hence the uncertainty in Δk was calculated using equation (13) where Q was replaced with the least count of the pixel tool.

Unlike the graduations, the method can be extended for the outer circles. Hence the measurements were taken for k = 2 (C_1, C_3, A_2, and B_2) as well as k = 3 (C_2, C_4, A_3, and B_3):

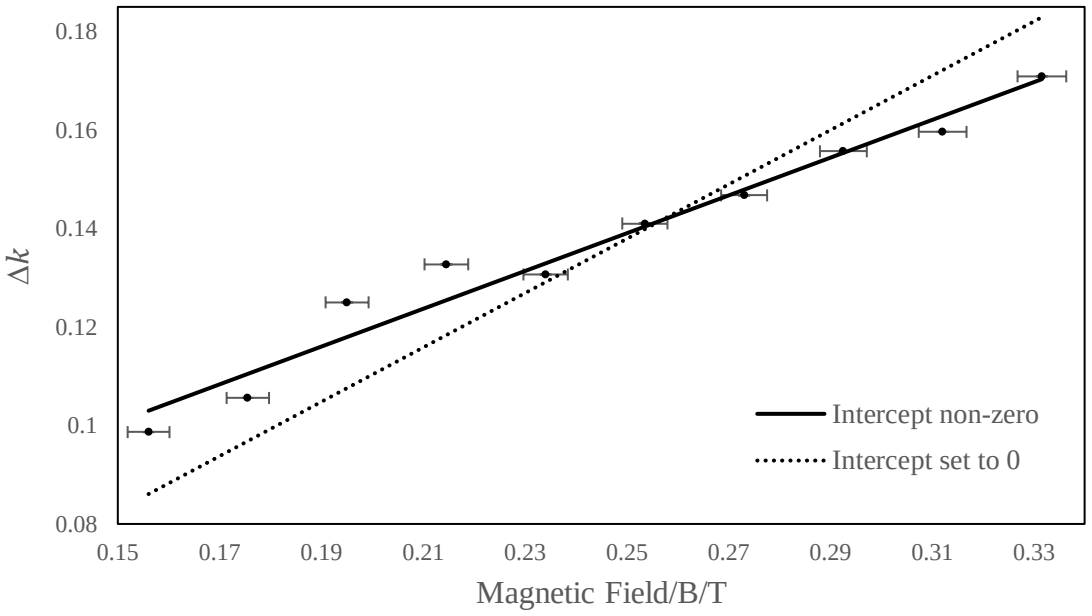

Figure 10: Data obtained from the pixel length (k = 2) plotted with Fractional Order Splitting (Δk) against Magnetic Field Strength. The two best fit lines were plotted with intercept fixed to 0 and not fixed, having R^2 = 0.9943 and R^2 = 0.9659 respectively (vertical error bars drawn but not visible).

Compared to the previous method of analysis, this method yielded smaller vertical error bars, however, it is still seen that some of the data points lie out of the general trendline.

The equations of the best fit lines of figure 10 were found through linest:

$$\Delta k = (0.38 \pm 0.03)B + (0.043 \pm 0.006)$$

$$\Delta k_{b=0} = (0.552 \pm 0.014)B$$

These were used to calculate the $\frac{e}{m_e}$ (using equation (14) and (15)) as:

$$\frac{e}{m_e} = (1.24 \pm 0.08) \times 10^{11}\ Ckg^{-1}$$

$$\left(\frac{e}{m_e}\right)_{b=0} = (1.78 \pm 0.05) \times 10^{11}\ Ckg^{-1}$$

Once again when fixing the intercept to 0, the value agrees with the theoretical value, having an error of 1.4% (calculated using equation (16)).

The data from the images when k = 3 is plotted below:

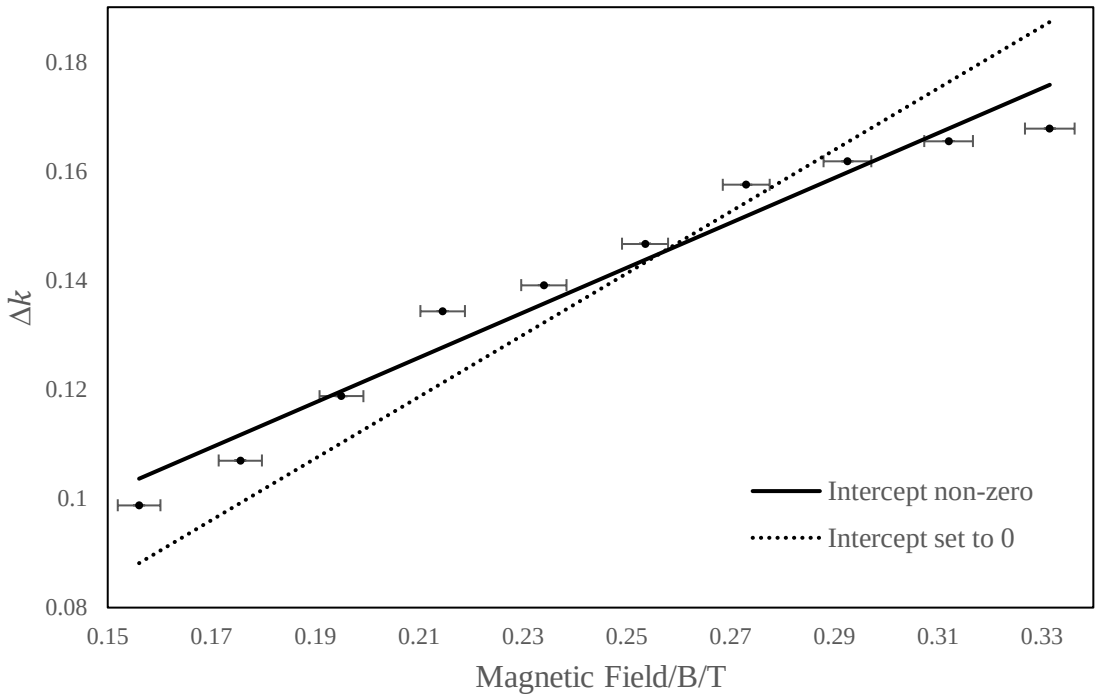

Figure 11: Data obtained from the pixel length (k = 3) plotted with Fractional Order Splitting (Δk) against Magnetic Field Strength, the two best fit lines were plotted with intercept fixed to 0 and not fixed, having R^2 = 0.9950 and R^2 = 0.9606 respectively (vertical error bars drawn but not visible).

The above plot has a lower correlation (when intercept is not set to 0) indicating lower precision compared to figure 10.

The equations of the best fit lines of figure 11 found through linest give:

$$\Delta k = (0.41 \pm 0.03)B + (0.039 \pm 0.007)$$

$$\Delta k_{b=0} = (0.565 \pm 0.013)B$$

These were used to calculate the $\frac{e}{m_e}$ (using equation (14) and (15)) as:

$$\frac{e}{m_e} = (1.3 \pm 0.1) \times 10^{11}\ Ckg^{-1}$$

$$\left(\frac{e}{m_e}\right)_{b=0} = (1.82 \pm 0.04) \times 10^{11}\ Ckg^{-1}$$

This clearly shows when intercept is fixed to 0, the value is closer to the theoretical value, however this value has the largest error, 3.8% (calculated using equation (16)) out of the three values calculated above. The source of errors in all three methods which are causing this effect will be discussed further in the next section.

IV Longitudinal Setup

The experimental setup was changed according to the bottom of figure 4 for the last part of the investigation. In this section, the images were only analysed qualitatively, since the produced Zeeman effect contains only the circularly polarized σ lines (which are visible due to the inclusion of the quarter-wave plate), preventing the calculation of $\frac{e}{m_e}$:

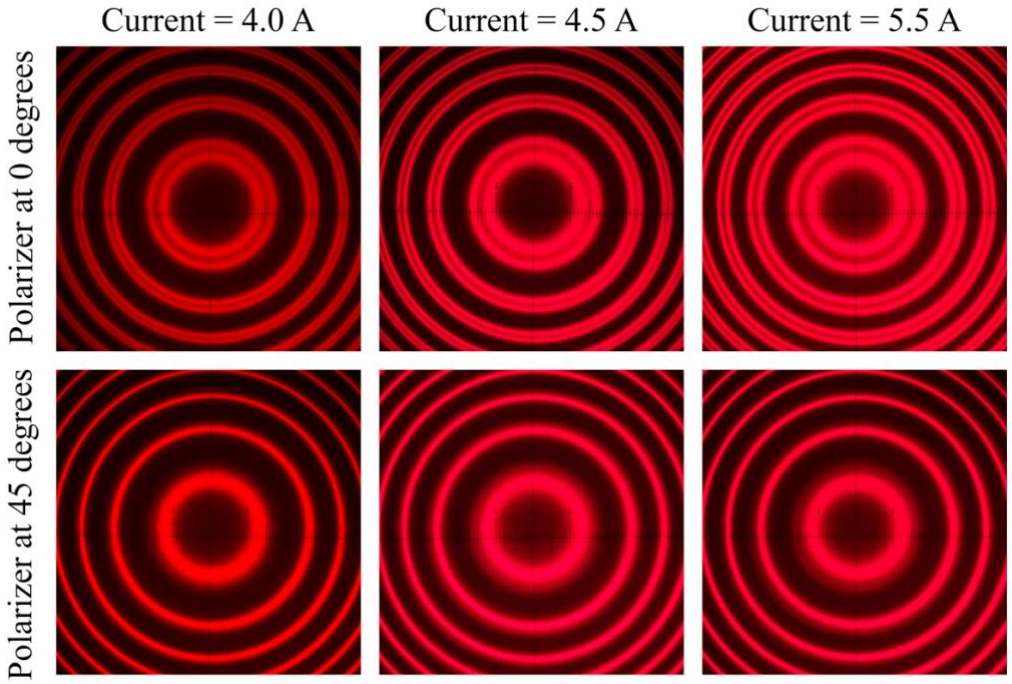

Figure 12: Overview of the images taken of the Zeeman effect for longitudinal configuration.

The above images show that the change in the interference pattern is visually negligible. However, when comparing the images with pixel measurements there is a noticeable difference which once again reveals the reason behind the large uncertainties when using the method of line graduations.

V Separation of Zeeman components

The separation of σ and π lines in frequency and wavelength ($\Delta\nu$ and $\Delta\lambda$) can be calculated using equation (6). $\Delta\nu$ was calculated for a few current values (4.0, 6.0, 8.5 A) and the theoretical value of $\frac{e}{m_e}$ was used:

$$\Delta\nu_{I=4.0A} = (2.18 \pm 0.06)\ GHz$$
$$\Delta\lambda_{I=4.0A} = (0.395 \pm 0.010)\ nm$$

$$\Delta\nu_{I=6.0A} = (3.28 \pm 0.06)\ GHz$$
$$\Delta\lambda_{I=6.0A} = (0.396 \pm 0.007)\ nm$$

$$\Delta\nu_{I=8.5A} = (4.64 \pm 0.07)\ GHz$$
$$\Delta\lambda_{I=8.5A} = (0.398 \pm 0.006)\ nm$$

Where the uncertainty was calculated using fractional uncertainty of the magnetic field and $\Delta\lambda$ was calculated using:

$$\Delta\lambda = \left|\frac{c}{f_0+\Delta\nu} - \lambda_0\right| \quad (17)$$

This shows that the change in wavelength is negligible for these increments of the current, indicating how large values of current changes are required for a noticeable change in the visual appearance.

4. Discussion

It is seen that the value of $\frac{e}{m_e}$ is much more accurate when fixing the intercept to 0 in all three methods. However, figure 9, 10 and 11, show this does not strongly correlate with the data and the intercept is significant as well (even if the R^2 is higher, this is due to the method of least squares which provides a higher value when the intercept is fixed).

This indicates a systematic error in the data which could be caused due to the tilt of the camera. As seen in figure 8, the images taken are slightly tilted, which impacts the distances recorded throughout the experiment. The camera was not disturbed throughout the experiment, hence all the data points have the same systematic error. This also indicates why the value is closer to the theoretical ratio when fixing the intercept to 0 (and the slope is larger), as this compensates for the systematic error present in the results.

Another error observed is the slight curve at the end data points seen in figure 11. This is due to the method of calculating the magnetic field. The values of magnetic field were extrapolated since the Zeeman effect was only observed clearly above 4.0 A of current. Above this value of current, the magnetic field may not necessarily follow a linear curve, causing this error. The effect is more pronounced for figure 11 since the measurement was done for $k = 3$, taking the curves near the edge which are more impacted by the magnetic field than the centre ring.

The investigation has also involved some random error due to guesswork involved in the line graduations method. There was also random error involved in the pixel measurement method as the brightness of the image varied the size of the edges of the Zeeman components, which could have caused the outliers observed in figure 10.

A major drawback for this experiment is the need for high current to generate the Zeeman effect. This prevented the calculation of specific cases of Δk ($\Delta k = \frac{1}{2}$ and $\Delta k = \frac{1}{3}$) and consequently $\Delta \nu$ using equation (6) and $\Delta \lambda$ between the σ and π lines for these values. These fractional order splitting require the σ and π lines to be equidistant for $\Delta k = \frac{1}{3}$ or σ overlapping with π lines for $\Delta k = \frac{1}{2}$:

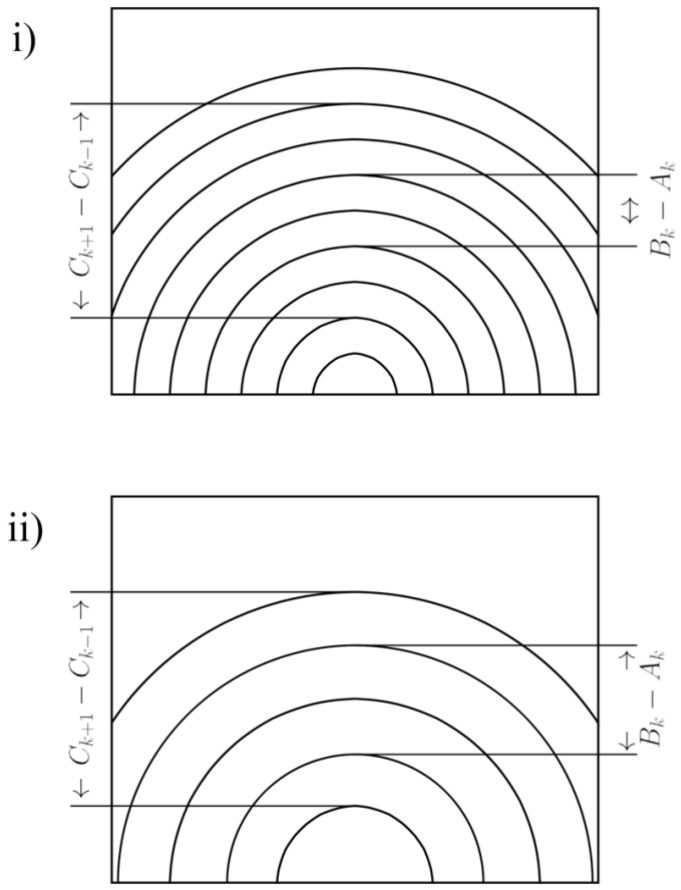

Figure 13: Theoretical diagram of the Zeeman effect when: i) $\Delta k = \frac{1}{3}$ and ii) $\Delta k = \frac{1}{2}$.

The above figure outlines how $\Delta \pi = 3\Delta \sigma$ and $\Delta \pi = 2\Delta \sigma$ for $\Delta k = \frac{1}{3}$ and $\Delta k = \frac{1}{2}$ respectively. This type of Zeeman effect could not be observed as it was found that 10.0 A was the current limit of the coils generating the magnetic field, and at this current supply the σ and π lines were not equidistant. The reason could be due to the degrading of the experimental equipment from prolonged use which may have decreased the power of the coils and thus the magnetic field as well. Hence, the analysis of the Zeeman effect could not be conducted on these special cases, limiting the scope of the experiment.

5. Conclusion

This experiment aimed to characterise the Zeeman effect of a Cadmium lamp in transverse and longitudinal configuration and calculate the value of $\frac{e}{m_e}$ from the data collected. With the setup used in this investigation, the Zeeman effect was observed and analysed effectively, out of which the best value of the ratio was found to be $(1.78 \pm 0.05) \times 10^{11}\ Ckg^{-1}$ having an error of 1.4%. The theoretical value lies within the uncertainty of the value.

Despite the seemingly high accuracy of the final value, it was still found that the experiment had several sources of error which could have been improved with; more observations, having a better setup for the camera mount (to avoid tilt) and calibrating the magnetic field for more values (by testing the range of current values for which Zeeman effect is visible, the calibration stage could involve those values as well).

In summary, the experiment obtained an accurate value of the ratio of elementary charge and the mass of an electron, however, has a few sources of errors which require improvements and may provide more accurate values.

References

1. King's College London (2024, 25 09), *"5CCP2100 Experimental Physics Laboratory Manual 2024/25"*. pg. 95-103

2. Tatum, J., (2024, 02 09). *"Stellar Atmospheres".* University of Victoria, Ch 7 Sec 21.

3. Jenkins, F. A., White, H. E., (1976). *"Fundamentals of Optics – Fourth Edition"*. D. P. Bhosale College, Koregaon, Ch 32 pg. 679-680.

4. Suzuki, M. S., Suzuki, I. S., (2011, 13 03). *"Zeeman effect in Na, Cd, and Hg"*. SUNY at Binghamton.

5. Hariharan, P., (1992). *"Basics of Interferometry"*. ScienceDirect, Ch 5 Sec 5.

6. LD Physics Leaflets (2024). *"Measuring the Zeeman splitting of the red cadmium line as a function of the magnetic field – spectroscopy using a Fabry-Perot etalon"*.

7. LD Didactic GmbH (2005). *"Instruction sheet 471 221*".

8. (2024). *"The NIST Reference on Constants, Units and Uncertainty"*.